Development of Foam Composites from Flax Gum-Filled Epoxy Resin

Corentin Musa, Mohammed Zaidi, Michaël Depriester, Yamina Allouche, Naïm Naouar, Alain Bourmaud, Dominique Baillis, François Delattre

Journal of
Composites Science

MDPI

Article

Development of Foam Composites from Flax Gum-Filled Epoxy Resin

Corentin Musa [1], Mohammed Zaidi [1,2], Michaël Depriester [3], Yamina Allouche [1], Naïm Naouar [2], Alain Bourmaud [4], Dominique Baillis [2] and François Delattre [1,*]

[1] UCEIV, UR 4492, Université du Littoral-Côte d'Opale, 59140 Dunkerque, France; corentin.musa@gmail.com (C.M.); medzaidi91@gmail.com (M.Z.); yamina.allouche@univ-littoral.fr (Y.A.)
[2] LaMCoS, INSA-Lyon, CNRS UMR 5259, 69621 Villeurbanne, France; naim.naouar@insa-lyon.fr (N.N.); dominique.baillis@insa-lyon.fr (D.B.)
[3] UDSMM, UR 4476, Université du Littoral-Côte d'Opale, 59140 Dunkerque, France; michael.depriester@univ-littoral.fr
[4] IRDL, UMR 6027, Université de Bretagne-Sud, 56321 Lorient, France; alain.bourmaud@univ-ubs.fr
* Correspondence: delattre@univ-littoral.fr; Tel.: +33-3-28-65-82-46

Abstract: In the present work, an innovative range of foams based on flax gum-filled epoxy resin was developed, reinforced or not by flax fibers. Foams and composites with different gum and epoxy resin contents were produced and their mechanical and thermal performances were characterized. To enhance the organic flax gum filler's cross-linking, we exploited the oxidized components' reactivity with the amine hardener (isophorone diamine). We compared the materials obtained with those derived from the native components. The flax gum and fibers were primarily characterized by chemical analysis, NMR, and FTIR to evaluate the mild oxidation of the native materials. The formation of chemical bonds between the oxidized polymer chains, epoxy resin, and hardener was evidenced by FTIR, and the materials were then studied by SEM and X-ray computed micro-tomography (CT) and submitted to mechanical and thermal tests. The relevance of the oxidation treatment was highlighted through a significant increase in density and mechanical performance (+36% and +81%, respectively, for the 100% flax gum material). The positive effect of the flax fibers on homogeneity evidenced through micro-CT analysis was also clearly addressed. This set of promising results paves the way for the future development of fully flax-based insulation composite materials.

Keywords: polymer-matrix composites (PMCs); molding compounds; flax gum; polysaccharide foam

Citation: Musa, C.; Zaidi, M.; Depriester, M.; Allouche, Y.; Naouar, N.; Bourmaud, A.; Baillis, D.; Delattre, F. Development of Foam Composites from Flax Gum-Filled Epoxy Resin. *J. Compos. Sci.* **2024**, *8*, 244. https://doi.org/10.3390/jcs8070244

Academic Editors: Deesy Gomes Pinto and Virupaxi Auradi

Received: 30 May 2024
Revised: 17 June 2024
Accepted: 21 June 2024
Published: 27 June 2024

1. Introduction

Today, the search for alternatives to petroleum-derived materials is an emerging topic in many fields of application, including furniture, boating, automotive, and aeronautics [1]. Agro-resources, more generally biomass, provide a wide range of renewable and biodegradable substances. These include wood and lignocellulosic plant fibers, plant polysaccharides (starch and its derivatives, chitin, etc.), proteins, and phenolic derivatives such as tannins [2]. Beyond their environmental benefits, the mechanical properties of lignocellulosic fibers such as flax or hemp are competitive with those of glass fibers [3]. Moreover, using bio-based polymeric materials to reinforce lignocellulosic fibers is a complementary and credible route to fully recyclable or degradable green materials.

Among the bio-based macromolecules, polysaccharides have multiple applications in the medical field [4] or food industry [5] and more generally for the development of materials [6]. These organic fillers used in the production of composites offer many advantages, including biocompatibility, biodegradability, chemical tunability, low density, high strength, and stiffness. Due to their versatility and interesting physicochemical properties, natural polymerics have gained attention to form foam materials for acoustic [7], thermal insulation [8], and biomedical applications [9]. These are solid, porous materials

formed from a range of open and closed cells that can be obtained by freeze-drying, gas formation using a blowing agent, three-dimensional printing, or melt extrusion. In these materials, the shape of the holes (open or closed) and the size of the pores, from micro- to macro-porous structures, affect the density, thermal conductivity, and acoustic performance of these biomass-based composites. In terms of design, the chemical composition and the control of the internal structure of the foams are therefore the criteria to be mastered when developing insulating materials. To improve their mechanical performance, polymeric foams can be strengthened by adding different natural fibers such as kenaf [7], bagasse [10], hemp [11], or jute and flax [12].

Among the cellulosic fibers, flax fibers have high mechanical properties [13], i.e., Young's modulus and strength at break, comparable to those of petroleum-derived materials [14]. An interesting way of developing new flax-based composites is adding polysaccharides from the seeds by an impregnation method as a matrix to obtain "wholly flax" bio-composites [15,16]. Flaxseed polysaccharides are water-soluble complex polymers with a highly branched structure [17] able to transfer stress into the composite with a maximal value of Young's modulus (E) and tensile strength (σ) for a 20% mucilage loading (w/w). In addition, it has been shown that mild oxidation of polysaccharides can be exploited to achieve a cross-linking reaction between the aldehyde groups of flaxseed gum and the epoxy resin components to form imine functions via a basic Schiff reaction [4]. This reactivity can be used to achieve cross-linking between the polymeric arms of the flax gum and the hardener present in the matrix. In addition, the carboxylic acid groups are also likely to form covalent intermolecular di-esters with hydroxyl groups at relatively low temperatures (70 °C) [6]. Finally, the combination of epoxy resins filled with oxidized polysaccharides has been shown to have an accelerating effect on curing, which represents an opportunity to increase the mechanical properties of polysaccharide-based bio-composites since as a nucleophile, the hydroxyl group can initiate the ring opening reaction of the epoxide group.

In addition to exploiting the reactivity of the various chemical groups, we propose to implement a freeze-drying process to prepare three-dimensional porous matrices. This process is widely used to form aerogels and foams for medical and food applications or composites manufacturing [18] by modulating and controlling the microstructure of materials through the ice crystals used as templates. In this context, our process for developing polysaccharide-based bio-composites in water can be particularly suitable for preparing porous structures, which could provide both light weight and stiffness to the materials. Given their advantages, we undertook to study their potential for i. the development of bio-sourced foams to create insulating biomaterials for the building industry and ii. thermo-molded formwork for the automotive industry.

In the present study, we prepared new foam composites based on flax fibers embedded in different formulations of native and oxidized flax gum matrices supplemented by epoxy resin to obtain stiff structures. This work aimed to study the potential of flaxseed gum as a composite matrix. Flax gum and flax fibers were oxidized under mild conditions by the TEMPO method in an aqueous solution to obtain aldehyde and carboxylic groups to exploit their reactivity with polysaccharides as well as epoxy resin and amine hardener to achieve efficient cross-linking. To this end, we prepared various mixtures in water of different epoxy resin/linseed gum ratios and analyzed the physicochemical properties of the resulting foams. In a second step, we prepared bio-composites by adding microfibrillated flax (MFF) to the mixture to observe its influence on the material structuring and property modulation. After the characterization of the mucilage and the modified fibers, the foams and bio-composites were characterized by X-ray computed tomography (X-ray CT). The thermal and mechanical properties of these new materials were evaluated.

2. Materials and Methods

2.1. Material and Reagents

Flax seeds and fibers (Damara variety) were produced commercially in North France (Van Robaeys Frères, France) and used as the raw materials.

2,2,6,6-Tetramethylpiperidine-1-oxyl radical (TEMPO, 98%) and sodium bromide NaBr (99%) were supplied by Merck and VWR Chemical companies, respectively. Sodium hypochlorite solution (12.5%) was purchased from Sigma Aldrich (St. Louis, MO, USA).

2.2. Oxidation of Flax Gum and Flax Fibers

The flax gum oxidation was performed by using TEMPO/NaOCl/NaBr according to the Kato proceeding [19]. A 5% mucilage solution was placed in a beaker and maintained at a temperature below 5 °C in an ice bath. TEMPO (0.01 mol per mucilage anhydroglucose unit) and sodium bromide (0.2 mol per mucilage anhydroglucose unit) were dissolved in 100 mL of water and then added to the flax suspension. The pH of the solution was adjusted to 10.75 with 0.5 M NaOH and then a 10% sodium hypochlorite solution (2 moles per AGU) was added to the mucilage solution. From there, the oxidation started and the pH was maintained at 10.75. The end of the reaction was indicated by pH stability and then the oxidation stopped. Then, the mucilage was precipitated by adding ethanol in a ratio EtOH/H_2O 3:1 (*V*:*V*). Finally, the precipitate was washed 3 times with water and then frozen at −80 °C and freeze-dried for 48 h at 0.2 mbar and 24 h at 0.001 mbar.

The oxidation of the flax fibers was adapted from the Sbiai protocol [20] and the oxidation of cellulose was done in batches of 250 g (1.54 AGU). The flax fibers were placed in a 5 L water bath retained below 5 °C and dispersed with an RW16 basic IKA mechanical agitator. Then, a mixture of TEMPO (0.01 mol per fiber AGU) and sodium bromide (0.2 mol per fiber AGU) was added to the fiber suspension. Sodium hydroxide and hydrochloric acid (1 M) were used to put the pH between 10 and 10.5 during the reaction. The end of the reaction was reached at pH stability (~8 h). The oxidation was stopped by adding ethanol to the solution in a ratio of 2.5 (V_m of fibers). The fibers were filtered and rinsed several times with distilled water, then the samples were frozen and freeze-dried.

2.3. Preparation of Flax Foams

For each sample, flax gum was first mixed with 160 mL of water and the solution was then left to stand for 12 h. The epoxy resin and fibers, if any, were then added to the polysaccharide solution to obtain 20% of organic matter in the mixture. The reticulation of the resin was obtained using a ratio of 2/3 of diglycidyl ether of bisphenol A and 1/3 of isophorone diamine (IPD). The formulations were then placed in a silicone mold and frozen at −80 °C before freeze-drying for 72 h at 2 mbar (primary drying) and 0.002 mbar for 24 h (secondary drying). After the freeze-drying proceeding, the samples were baked at 80 °C for 5 h in the oven. Finally, they were polished to obtain 20 mm high cylinders with 43–45 mm diameters with parallel top and bottom faces.

The nomenclature chosen to name the flax gum (FG) foam samples is FG-X, which is the rate of FG and the remaining fraction corresponding to the epoxy resin content (for example, FG-20 corresponds to 20% of mucilage added to 80% epoxy resin). The index "ox" is used to note oxidized samples. The composites were made from 12% flax gum, 48% fiber, and 40% epoxy resin (FG-Comp from native materials FG and fibers, FGox-Comp from oxidized materials FGox and Fox).

2.4. Characterization

The foam and composite samples were characterized by scanning electron microscopy (SEM) under high vacuum with a field emission SEM instrument (JSM-7100F, Tokyo, Japan). Coatings of the samples were applied with a thin (around 10 nm) layer of chromium before observation.

The differential scanning calorimetry (DSC) thermograms were recorded on a DSC Q1000 DSC instrument (TA instruments, New Castle, DE, USA). An indium standard was used for the calibration and nitrogen was used as the purge gas. The sample was heated from room temperature to 300 °C at a heating rate of 10 °C/min. SDT Q600 (TA Instruments, New Castle, DE, USA) was used for thermogravimetric analysis (TGA). Around 4–8 mg

samples were scanned from 20 to 800 °C at a heating rate of 10 °C/min in the presence of 100 mL/min nitrogen flow.

The ATR-FTIR spectra of the precursors were recorded on a Perkin Elmer Spectrum BXII spectrometer over the wavenumber range of 500–4000 cm^{-1} with a resolution of 1 cm^{-1}. NMR spectra were recorded on a Bruker Ascend^{TM} 400 MHz NMR spectrometer at room temperature and D_2O was used as solvent.

The neutral sugar composition was determined by colorimetric methods [21]. The acidic sugar content was calculated as milligrams of D-galacturonic acid per milligrams of the mucilage [22] (Table 1).

Table 1. Carboxylate and aldehyde contents of the native flax gum (FG), flax fiber, oxidized flax gum (FGox), and oxidized flax fiber (ox. Fiber).

	Carboxylate (mmol/g)	Aldehyde (mmol/g)		Carboxylate (mmol/g)	Aldehyde (mmol/g)
FG	0.59 ± 0.01	1.64 ± 0.45	Fiber	1.25 ± 0.15	3.41 ± 0.03
FGox	1.13 ± 0.32	2.56 ± 0.55	Ox. Fiber	2.46 ± 0.08	4.60 ± 0.04
Rox	1.90	1.56		1.97	1.35

Bulk density measurements (Table 2) were performed using an Electronic Digital LCD Gauge Stainless Nonius Caliper Micrometer 150 mm 6-inch MIS and a VWR LP 3102 balance.

Table 2. Quantitative analysis of the density and porosity of FG and FG-filled epoxy resin composites.

Sample	Density ($kg \cdot m^{-3}$)	Section Indent (%)	Porosity * (%)	Sample	Density ($kg \cdot m^{-3}$)	Section Indent (%)	Porosity * (%)
FG-100	228.9 ± 9.3	9.8	68 ± 2.4	FGox-100	311.4 ± 3.4	13.0	69 ± 1.1
FG-80	231.7 ± 8.2	7.9	68 ± 2.5	FGox-80	286.0 ± 5.6	11.9	73 ± 1.1
FG-20	219.5 ± 3.0	5.6	61 ± 3.0	FGox-20	236.7 ± 4.7	7.6	79 ± 1.1
FG-Comp	194.4 ± 5.3	0.1	65 ± 1.1	FGox-Comp	209.4 ± 2.5	0.6	67 ± 1.1

* From 2D cross-sectional image according to the ratio of the sum of the dark pixels identified to the total number of pixels.

The composite materials underwent microstructural characterization through X-ray computed micro-tomography (CT) and image analysis to assess changes in microstructure as a function of composition and oxidation treatment. X-ray scans were operated at a voltage of 60 kV and a current of 160 µA. The data acquisition system recorded 1120 projections distributed over 360° along the vertical axis of each specimen. The projections were reconstructed using a cone-beam filtered back-projection algorithm [23] and this process was implemented in the X-ACT 2.0 software (RX Solutions, Boynton Beach, FL, USA). For each sample, four representative elementary volumes (REVs) of about 10 mm^3 were selected and subsequently analyzed to calculate the porosity and volume fractions of the different components within the composites. The pixel size for image scanning was 8 µm. This resolution was selected to optimize both the quality and number of scans.

Image pre-processing was carried out using the open-source ImageJ 1.54 software [24], and segmentation was performed using the LABKIT plug-in [25]. Porosity within the samples was calculated by dividing the volume of the segmented component by the total volume of the REV, and then the average porosity was determined [26]. Note that, during the image analysis, pores and flax fibers in contact with the edges of the REV were excluded from the calculation to avoid their underestimation.

Compression tests were performed on the composites with an MTS Synergie RT/1000 system (MTS, Eden Prairie, MN, USA) at a controlled temperature of 296 K and a relative humidity of 48%. The crosshead displacement speed was 2 $mm \cdot min^{-1}$ according to ASTM D1621 norm [27]. The sample was compressed into the 20% thickness of the original.

Experimental thermal effusivity and conductivity of the materials were obtained by using a Thermal Conductivity Analyzer (TCi) supplied by C-Therm Company (Fredericton, NB, Canada). This device uses the non-destructive Modified Transient Heat Source (MTPS) method (Conform to ASTM D7984 [28]). Thermal conductivity values between 0 and 10 $W \cdot m^{-1} \cdot K^{-1}$ can be measured. All experiments were repeated five times and realized at room temperature.

3. Results

3.1. Characterization of Flax Products Following TEMPO Oxidation

First, to quantify the chemical modification of the flax gums and fibers following the TEMPO oxidation process, the determination of the acid and aldehyde functions on the different materials was performed before freeze-drying and shaping of the foams (Table 1). The carboxylate aldehyde contents of flax gum (FG) are due to its D-galacturonic acid and hemiacetal forms. The chemical oxidation of polysaccharides resulted in a more significant increase in acid function concentration (Rox = 1.9) relative to aldehyde content (Rox = 1.56). Modification of the fibers gave results comparable to those obtained on the gum with a more important conversion in acid function. As expected, these results are consistent with the mild oxidation of flax products.

The native and modified flax gum and fibers were then characterized by NMR and FTIR experiments to confirm the chemical modifications resulting from the oxidation. The ^{1}H and ^{13}C NMR spectra of the flax gum and oxidized flax gum are shown in Figure 1. The ^{1}H NMR spectrum of the flaxseed gum can be divided into three zones corresponding globally to the signatures of the amino acids between 0 and 3 ppm, polysaccharides from 3 to 6 ppm, and phenolic compounds and acids beyond 6 ppm. The examination of the ^{1}H NMR resonances of the native flaxseed gum demonstrates the presence of amino acids by the characteristic peaks of alanine and linustatin (at 1.48 and 1.71 ppm, respectively), which were removed following the oxidation. In contrast, the intensity of the peaks corresponding to the non-bound acids (acetic and formic acids) and neutral polysaccharides (Ara: 5.13, Xyl: 3.49; 3.42, Gal: 3.77; 3.56; 3.47 ppm) and acids (Rha: 3.84, 3.78; 1.26/16.7, GalA: 4.42; 3.89) increased after oxidation. However, apart from the resonance of the formic acid at 8.46 ppm resulting from the pectine oxidation [29], the ^{1}H NMR spectra do not detect the oxidation of primary hydroxyls.

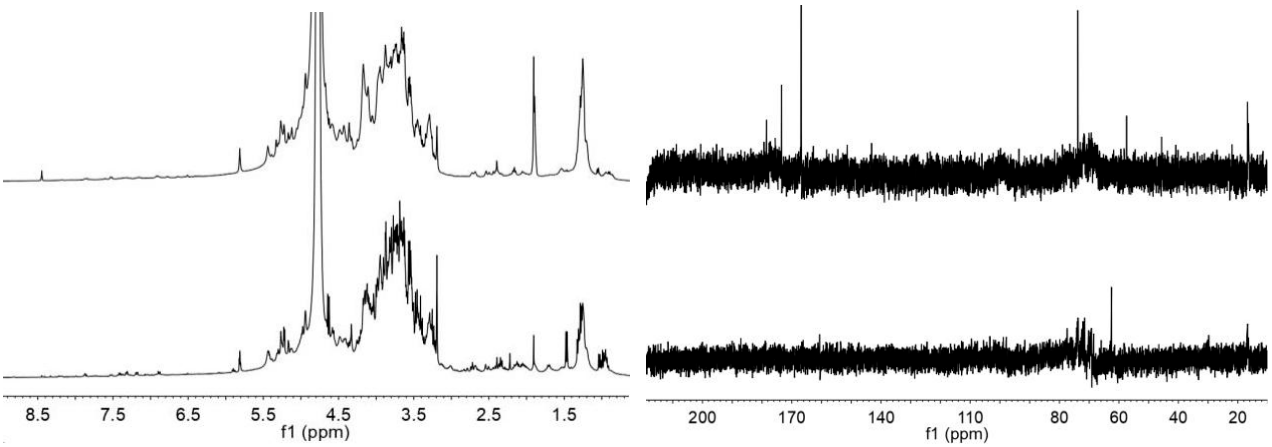

Figure 1. ^{1}H and ^{13}C NMR spectra of oxidized flax gum (top) and native flax gum (bottom).

The ^{13}C NMR spectrum of native flax gum is similar to those previously reported and agrees with a polysaccharide composition [30]. The spectral zone from 60 to 110 ppm includes all of the carbons of ether oxide and the aliphatic groups present in the polysaccharide rings. After oxidation by the TEMPO procedure, despite a lack of sensitivity in the aliphatic carbon region, new resonance signals appeared beyond 140 ppm, which is characteristic of the formation of oxidized functions. The transition at 166.9 ppm corresponds

to the metabolization of formic acid, which is consistent with the ^{1}H NMR spectra. Both resonances 173.1 ppm and 188.2 ppm can be attributed, respectively, to acid and aldehyde functions from the oxidation of the C6 primary hydroxyl groups. As expected, the mild synthesis conditions resulted in incompletely oxidized products leading to the formation of aldehyde or hemiacetal and acid groups.

The qualitative analysis of the native flax products (extracted flax gum and fibers) by FT-IR is presented in the Figure S1A. Whether native or oxidized, the gum samples show the general characteristics of the absorption bands of polysaccharides. The vibrations of the -OH groups correspond to the stretching bands of the broad and intense signals centered around 3300 cm^{-1}. The C-H stretching band of polysaccharides was observed at 2921 cm^{-1}. The vibrations band at 1412 cm^{-1} is attributed to the carboxylate (COO^{-}) and free carboxyl groups (rhamnogalacturonan and homogalacturonan) [31]. The shoulders observed at 1345 cm^{-1} for FG-100 and 1323 cm^{-1} for FGox-100 can be correlated to the wagging vibrations of –OH. The carbonyl groups of the acidic and aldehyde groups from poly-galacturonic acid exhibit a strong and large absorption band at 1598 cm^{-1} and 1243 cm^{-1} [32]. Finally, other characteristic peaks representative of multiple –C–O– stretching due to –OH and carbonyl groups are evidenced through the largest bands between 1175 and 840 cm^{-1} [33]. Comparison of the oxidized mucilage and neutral species spectra demonstrates a strong change in the ratio of band intensities associated with C–O elongations, which are consistent with the increase in the concentration of oxidized groups after TEMPO treatment. Regarding the fiber oxidation (see Figure S1B), the FTIR spectrum of oxidized fiber shows an increase of absorption at 1604 cm^{-1} compared to the untreated fiber, which exhibits a weak band at 1622 cm^{-1}.

3.2. Characterization of Flax Gum Foams and Composites

The FTIR investigations of flax gums foams FG-100 and FGox-100 and flax gum-filled epoxy-filled foams FG-80 and FG-20 are shown in Figure 2. These reports aim to highlight the chemical modification of the flax gum and characterize the interactions between the polysaccharides and the epoxy resin.

FG-100 foam shows two carbonyl stretching vibration peaks at 1634 cm^{-1} and 1538 cm^{-1} characteristic of acid residues. The shoulder at 1435 cm^{-1} indicates the bending vibration of N=C and ethylenic bonds due to the imide bond formed between the polymeric chains and the amino acids still present in the native mucilage [34]. For FGox-100, the characteristic peaks of –COO– stretching, CH_2 bending, and C–O–C stretching bands are shifted from 1411 to 1406 cm^{-1}, 1318 to 1325 cm^{-1}, and 1017 to 1028 cm^{-1}, respectively. These absorption band shifts could be attributed to the carboxylic moieties linking with adjacent saccharides to form a crosslinked network. As expected, the FTIR spectra of materials containing epoxy resin and hardener fractions (Figure 2B and Figure S2 in Supplementary Materials) show the appearance of new absorption bands at 1510 cm^{-1}, 1451 cm^{-1} and 1242 cm^{-1} due to epoxy resin. The peaks at 825 cm^{-1} and 752 cm^{-1} were attributed to the C–O stretching of ether groups as a result of the opening of the epoxy rings reacting with the hemiacetal groups from the aldehyde and hydroxyl of the flax gum [35]. This consideration is well reflected on the FTIR spectra of the materials with high epoxidation rates (FG-20), showing a strong increase in the C–O elongation bands at 1182 cm^{-1} and 1102 cm^{-1} (the strong peak at 1030–1035 cm^{-1} is relative to the carbohydrate C–O functions). Finally, the hemiacetal formations resulted in a decrease in OH absorption bands around 3350 cm^{-1}. Otherwise, the IR spectra of the two composites (Figure S2B in Supplementary Materials) show the same absorption bands as the epoxidized foams and do not distinguish any specificities. It can therefore be assumed that the reactivity of the different components has not been affected compared to non-fibrous materials.

The microstructure and some physical parameters of the thermoset moldings were deeply examined. First, the foams and composite thermosets are shown in Figure 3 to evaluate their macromorphological aspects, and the density, section indent, and porosity of the materials are listed in Table 2. To the naked eye, the oxidized samples show a lighter

coloration, ranging from light brown to beige due to the bleaching of the mucilage and fibers following the TEMPO process. It should be noted that some defects can be observed on the surface and outer edges of the cylinders, particularly on the untreated samples. These defects are mainly due to the high viscosity of the mixtures, which leads to molding problems. The oxidized mucilage is therefore more fluid, enabling the formation of more homogenous cylinders and limiting the production of gaps. The foams all have a more or less pronounced external porosity, which increases concomitantly with the resin content and, therefore, inversely with the flax gum content of the samples.

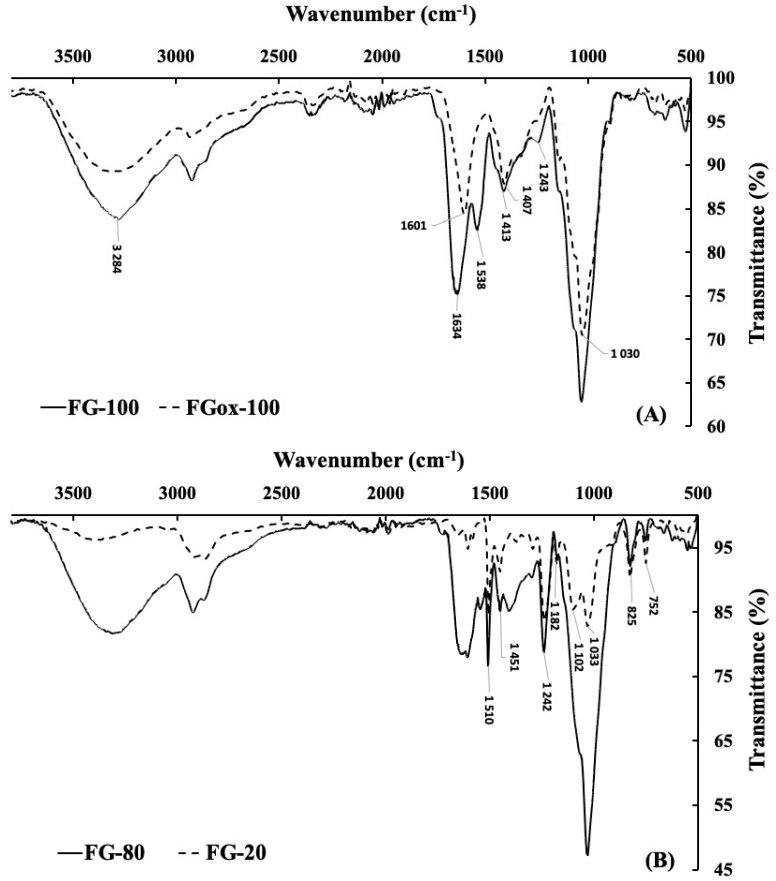

Figure 2. FTIR spectra of (**A**) flax gum foams (FG-100 and FGox-100), (**B**) flax gum-filled epoxy-filled foams (FG-80 and FG-20).

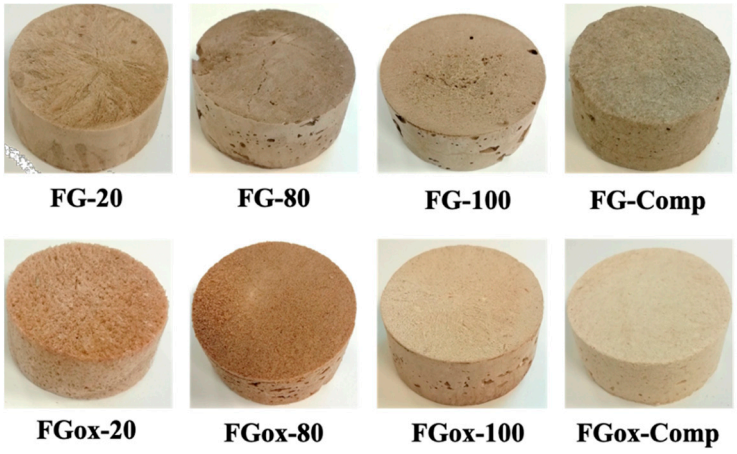

Figure 3. Pictures of thermoset flax gum foam and composites FG-Comp and FGox-Comp.

Table 2 shows the density of the mucilaginous foams and composites and their section indent. The density of the foams exhibits a drop when the mucilage content is reduced, most notably for the oxidized samples with a reduction of 24% of the density from 100% to 20% against a decrease of 4% for the non-oxidized foams. This result is consistent with the cross-section area after molding shrinkage (section indent), which is larger for the oxidized samples and can be attributed to the intramolecular networks formed between the flax gums, epoxy resin, and amino-hardener.

For both composites named FG-Comp and FGox-Comp, the bulk density is greatly reduced due to the high fiber content (48%), and they have a very low sectional shrinkage due to the high resin content (40%), which stiffens the materials. The results of the porosity calculated from the X-ray CT images shows two distinct trends: on the one hand, a slight decrease in porosity according to the density loss for natural gum-based samples, and on the other hand, an opposite trend for the oxidized samples, which show a significant increase in porosity with a decrease in density. These results are probably due to the different textures of the samples, depending on the nature of the material (natural or oxidized) and the gum/resin ratio.

The SEM-observed cross-section morphologies of the foams are shown in Figure 4 and in the Supplementary Materials (Figure S3). The two FG-100 samples show an alveolar structuring due to water extraction during the directional freeze-drying process along the *z*-axis. For these materials, the empty cells appear larger and less numerous for the natural gum foam than for the oxidized ones with sizes of 70–100 µm and 40–80 µm for FG-100 and FGox-100, respectively. The introduction of 20% resin (FGox-80) results in a network that appears less open than for the fully mucilaginous foams. The oxidized gum FGox-80 shows inclusions that could be due to a poor mixture between the resin and the polysaccharide chains. At 80% resin content, the foams are structured by a lamellar network sheet form, well-formed and uniform for FG-20 with an interlamellar distance of around 100 µm. For FG-20 and FGox-20, a reduction in density is observed, while the porosity of the former decreases and that of the latter increases, suggesting that the internal structures of the two foams are different.

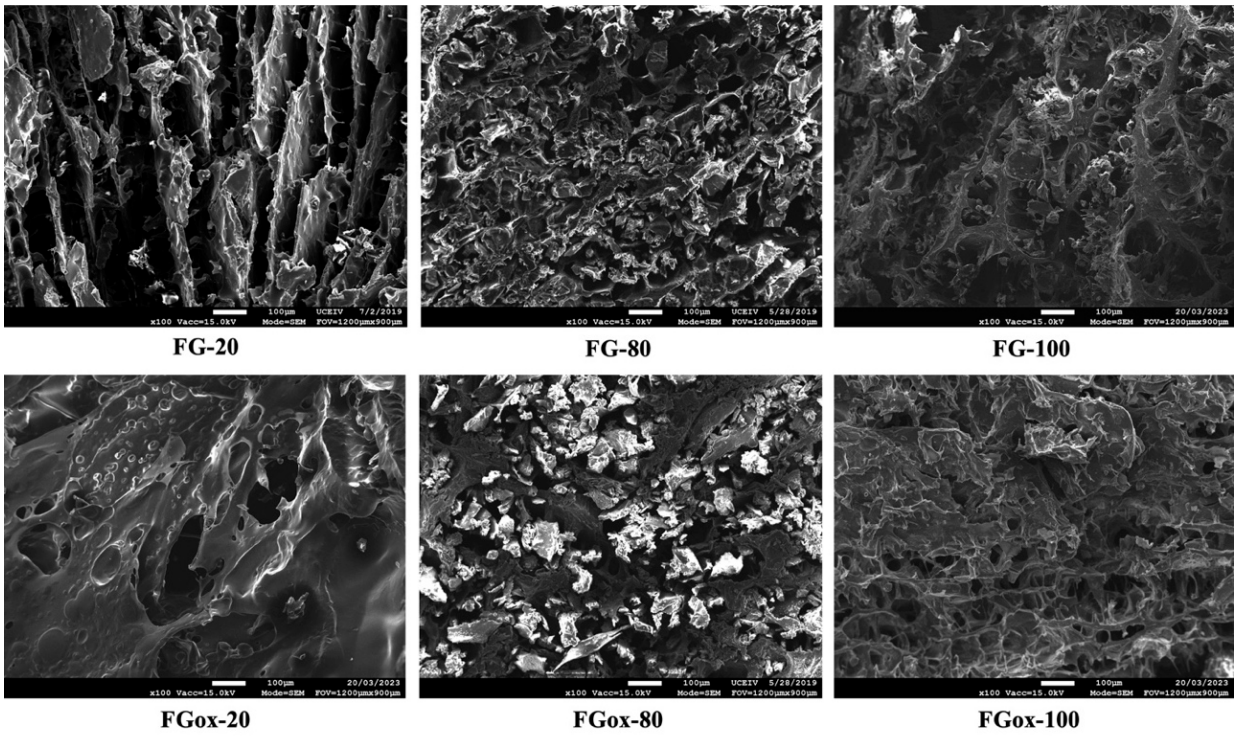

Figure 4. SEM images of the cross-section morphology of flax gum foams.

For FGox-20, the material is not as well aligned along the lyophilization axis and appears non-homogeneous in its structuring with less organized lamellae to FG-20. These observations on the texture of the materials show a difference in reactivity between the epoxy precursor and the amine hardener due to the least compatibility of the oxidized mucilage with the resin compared to the natural mucilage. The observation of the composites does not provide any notable differences between those obtained from natural or oxidized components (see Supplementary Materials). In both cases, we distinguish the fibers mixed with the mucilaginous fraction, forming a coating around the fibers and resulting in similar porosities.

The micro-CT pictures of Figure 5 show the microstructures and pore morphologies of the native and oxidized flaxseed gum/epoxy composites for the different fractions of FG. The porosity degree and density change from 61 to 65% and 194 to 228 kg/m^3, respectively. It is challenging to compare our data with literature values due to the huge diversity in processing and biobased components used by authors. Only poor data exist about the porosity degree, but the density can be compared, which is indirect information. For example, for jute- and flax-reinforced starch-based composite foams [12], a density from 214 to 336 kg/m^3 was reported, and for eucalyptus pulp foam, Ferreira et al. measured [36] densities between 150 and 180 kg/m^3, in good agreement with our data. In our case, the different observations made on foams and composites highlight that the porous network of the matrix is interconnected and open with three types of pores: (i) inter-lamellar pores, with an average distance between adjacent lamellae that varies from 2 to 300 µm; (ii) spherical and sub-spherical globular pores originating from air trapped in the matrix during the manufacturing process, with an average maximum diameter below 1500 µm; and finally, (iii) micro-cracks developed by the relaxation of thermal stresses during freezing, having the same orientation as the interlamellar pores.

For the native matrices FG-100, FG-80, and FG-20, the images show that the structure is organized lamellae and porous structures as previously seen in the SEM experiments. Similar architectures were observed in the graphene/epoxy composites and in porous ceramic where the parallel alignment of the lamellae is due to the extraction of freeze-dried ice crystals in the vertical direction of the specimens [37,38]. As evidenced in Figure 5E, the lamellar structure of FG-20 is more structured and long-range compared to FG-80 and FG-100, which show more and more defects and cracks as the mucilage content increases. These defects are consistent with the difficulty of processing due to the viscosity of the natural mucilage and it provides additional pathways for fluid flow in the matrix, resulting in a higher overall porosity.

The pore network of the oxidized flax gum exhibited significant changes compared to the native flax gum, as shown in Figure 5B, Figure 5D, and Figure 5F, respectively. These matrices appear to be highly porous, rough, and irregular. Although its mucilage fraction was smaller, the interaction of epoxy with 20% of oxidized mucilage allowed greater disorder of the matrix, resulting in an incompatible appearance and some cracks compared to FG-20 (Figure 5E,F) to give 61% and 79% of porosity for FG-20 and FGox-20, respectively. When increasing the mucilage fraction in the matrix, the samples had a more homogeneous appearance, and the pores became relatively homogeneous (Figure 5B,D), which could contribute to their better mechanical properties [39].

Introducing flax fibers into the flax gum significantly changed the microstructure of the untreated and oxidized composites, as shown in Figures 5G and 5H, respectively. The pores in the composite are almost spherical and more homogeneous, indicating good compatibility between the flax fibers and the matrix, reinforcing the cohesion and homogeneity of the system. Indeed, the absence of cracks or deformations in the composite is a positive indication of its structural integrity.

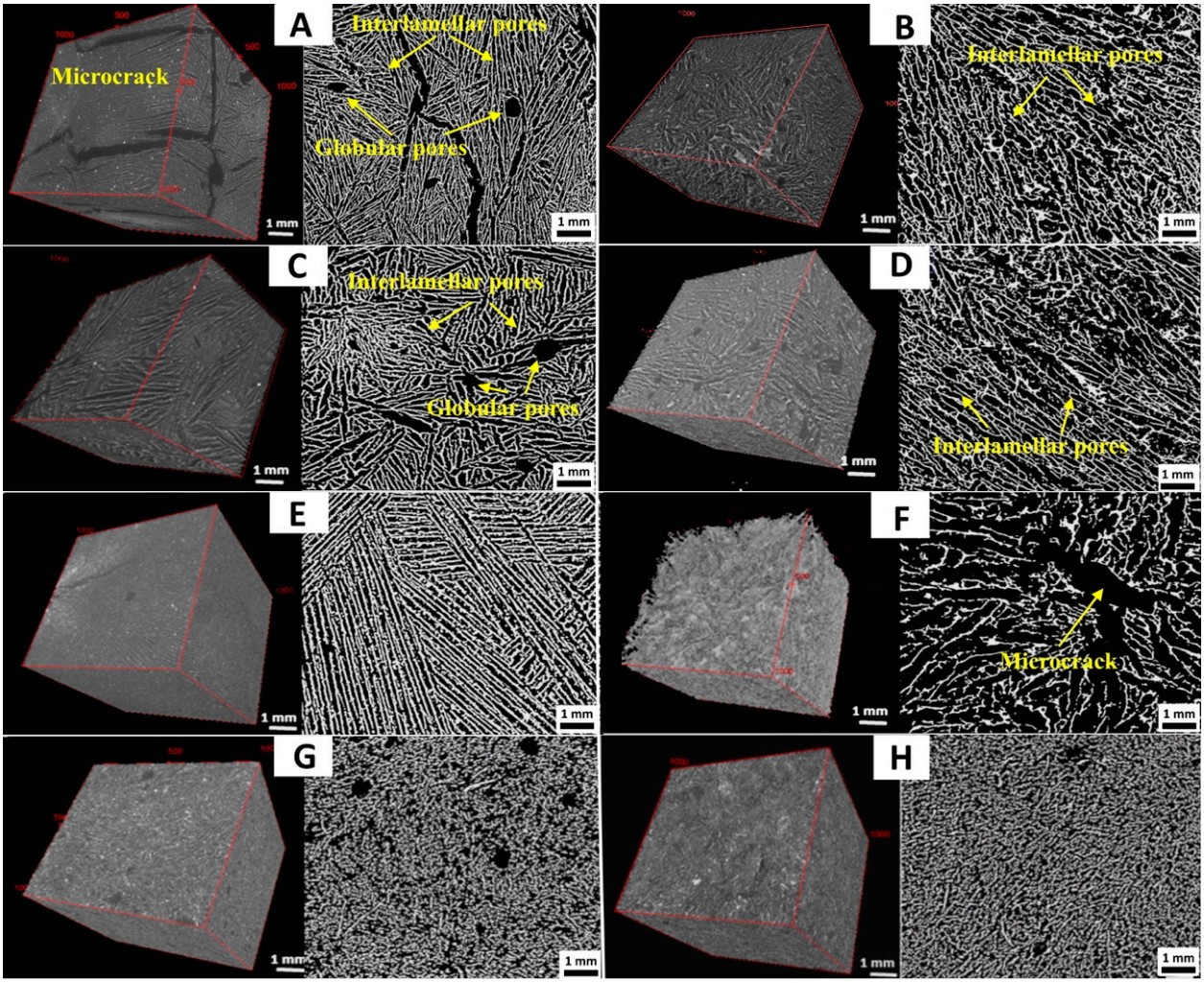

Figure 5. Pictures and micro-CT analysis of flax gum/epoxy and composites represented in 2D slices and 3D reconstructions of cubic subvolumes of the same REVs of FG-100 (**A**), FGox-100 (**B**), FG-80 (**C**), FGox -80 (**D**), FG-20 (**E**), FGox-20 (**F**), FG-Comp (**G**) and FGox-Comp (**H**).

3.3. Mechanical Analysis of Flax Gum Foams and Composites

Compression tests of the initial specimen height were performed on the mucilaginous composites to analyze the in-service damages. The data are synthesized in Table 3; once again, as explained for the density values, a comparison with literature value is not facilitated by the diversity of the process and components while a compression test is commonly used on biobased foams.

Table 3. Mechanical properties of flax materials.

Sample	E_c [a] (Mpa)	σ_{10} [b] (kPa)	Sample	E_c [a] (Mpa)	σ_{10} [b] (kPa)
FG-100	10.6 ± 1.2	742 ± 100	FGox-100	19.2 ± 0.4	1275 ± 28
FG-80	14.9 ± 2.3	784 ± 110	FGox-80	11.9 ± 2.0	722 ± 52
FG-20	11.8 ± 0.5	721 ± 9	FGox-20	10.3 ± 1.5	654 ± 39
FG-Comp	5.6 ± 0.1	352 ± 1	FGox-Comp	10.1 ± 0.6	454 ± 28

[a] Rigidity against the collapse of microscopic cavities; [b] Stress at 10% strain.

Our values are in the same range as data obtained on biobased isocyanate PU by Valette et al. [40] and Peyrton et al. [41] with compressive stress ranging from 0.1 and 0.5 MPa and a modulus between 12 and 63 MPa. On malt bagasse/cassava starch degradable composite systems, another research team demonstrated stress between 11 and 18 MPa [10], which is also in good agreement with the values of the present paper.

Figure 6 shows the compression curves at 20% of 20 mm thick flax gum rigid foams including two distinct gradients. In the first part, the load deformation curve has a constant slope, corresponding to the elastic deformation region and the higher compression modulus domain of the material. Then, the increase in deformation leads to damage, the rigid foams and composites no longer being able to support the load. From this level of compression, the network of interconnected pores collapses into an agglomerated matrix.

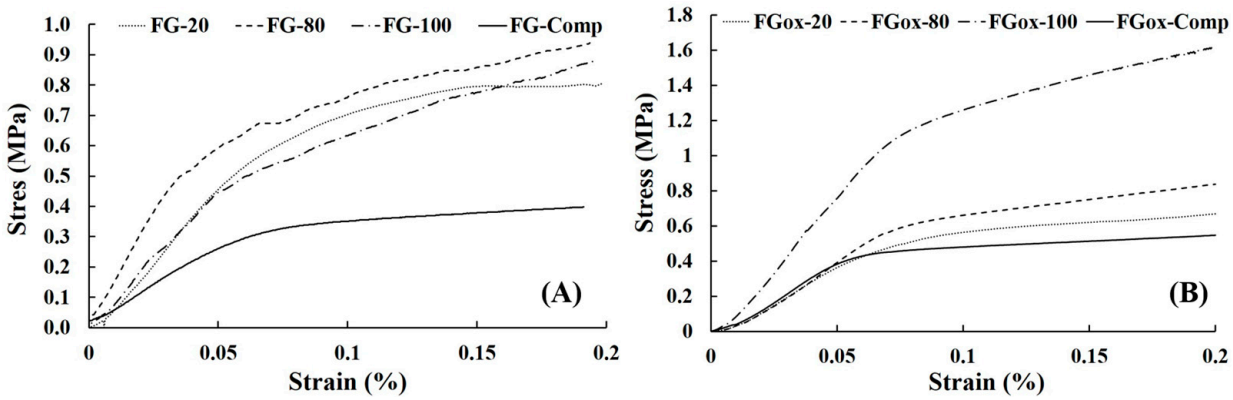

Figure 6. Stress vs. strain curve of flax materials obtained from native flax gum (**A**) and from oxidized flax gum (**B**).

The examination of the results shows that the FGox-100 foam, which has the highest density, is also the most resistant and that all of other materials give similar results. This significant difference is due to the important curing effect obtained with the oxidized gum, which reinforces the mechanical properties of the FGox-100 foam compared to the FG-100. Furthermore, the better textural homogeneity of FGox-100, which does not present fractures like its counterpart FG-100, is consistent with its high mechanical properties.

Introducing 20% epoxy resin into the mucilaginous matrix strongly reduces the mechanical strength of the oxidized gum FGox-80, while the opposite effect is observed for the native gum FG-80 (Table 2). This is probably due to a lack of miscibility between the components as evidenced by the SEM pictures, which show some resin inclusions in the flax gum matrix (see Supplementary Materials). In addition, when epoxy resin is predominantly introduced (FG-20 and FGox-20), the effect of the gum is significantly reduced, resulting in materials with similar mechanical performance. Finally, the results obtained for FG-Comp and FGox-Comp (48% fibers, 12% flax gum, and 40% epoxy resin) show that the oxidized composite has almost identical mechanical properties to the foams while the use of original non-oxidized components results in a decrease by a factor of two in their mechanical performances. This is consistent with the greater textural homogeneity of the composite system, highlighting again the miscibility of the components of FGox-Comp. The macromorphological analysis of the fracture profiles of the composites at 10% strain (Figure 7) shows spalling and heavy fracturing of the non-oxidized materials. The oxidized materials appear to be more cohesive and more likely to resist compression.

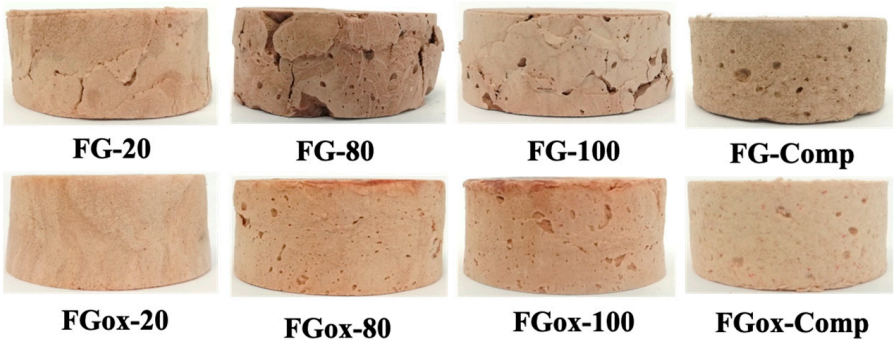

Figure 7. Fracture profiles of flax materials.

3.4. Thermal Properties of Flax Gum Foams and Composites

Thermal conductivity depends on many factors: the phase of a material (solid, liquid, gas), its chemical content and structure, the interfaces between phases/components, the presence of porosities, and their shapes [42]. Values of the thermal conductivity of the flax gum FG-100 (0.054 ± 0.001 $W \cdot m^{-1} \cdot K^{-1}$) are consistent with the ones reported by other authors for similar systems (Table 4) [43].

Table 4. Thermal parameters of foam based on flax mucilage.

Sample	Conductivity $W \cdot m^{-1} \cdot K^{-1}$	Diffusivity m^2/s
FG-100	0.054 ± 0.001	$(1.53 \pm 0.07) \cdot 10^{-7}$
FG-80	0.065 ± 0.001	$(1.40 \pm 0.09) \cdot 10^{-7}$
FG-20	0.057 ± 0.001	$(1.45 \pm 0.06) \cdot 10^{-7}$
FG-Comp	0.064 ± 0.001	$(1.40 \pm 0.05) \cdot 10^{-7}$
FGox-100	0.082 ± 0.001	$(1.42 \pm 0.07) \cdot 10^{-7}$
FGox-80	0.095 ± 0.002	$(1.53 \pm 0.06) \cdot 10^{-7}$
FGox-20	0.041 ± 0.001	$(2.55 \pm 0.17) \cdot 10^{-7}$
FGox-Comp	0.078 ± 0.001	$(1.40 \pm 0.07) \cdot 10^{-7}$

Non-oxidized and oxidized flaxseed gum/epoxy materials have very dissimilar thermal conductivities. Non-oxidized ones have thermal conductivity values ranging between 0.054–0.065 $W \cdot m^{-1} \cdot K^{-1}$ and the oxidized ones (except FGox-20) have values between 0.082–0.095 $W \cdot m^{-1} \cdot K^{-1}$. These differences can be explained mainly by the higher densities and lower porosity values for the oxidized samples compared to the non-oxidized ones, while the shape of the pores has a negligible effect, as shown when the thermal conductivity values are compared with the porosity shapes depicted by the micro-CT images (Figure 4). The FGox-20 exception (thermal conductivity of 0.041 $W \cdot m^{-1} \cdot K^{-1}$) can be explained by the high porosity of the matrix ~79% (Cf. Table 2) caused by the opening of the pores and the development of microcracks during curing (Figure 5F). Mucilage (oxidized or non-oxidized) can also affect the overall thermal conductivity, but this should be less predominant than its induced effect on the sample density and porosity. This explanation is substantiated by a recent article [26] on the modeling of effective thermal conductivity of structures composed of flax gum (FG-100) and epoxy resin. Porosity proved to be the predominant factor influencing the effective thermal conductivity of samples as a function of the mucilage/epoxy ratio. The composites showed the same trends as their corresponding flaxseed gum materials, with the thermal conductivity of FG-Comp being lower than that of FGox-Comp. For both non-oxidized and oxidized flaxseed gum materials, the incorporation of 20% epoxy resin leads to an increase in the thermal conductivity whereas a decrease is observed at 80%

epoxy introduction. Overall, the variation in thermal diffusivity depends on the flax gum filler. A decrease is observed as the thermal conductivity increases for native mucilage, while an opposite trend is found for oxidized polysaccharides. This result highlights the difference in the internal pore network structure between the two types of material. Based on these results, it can be inferred that the native-based matrix materials (FG) may be more suitable for thermal insulation applications than the oxidized-based matrix materials (FGox) due to their lower effective thermal conductivity values.

4. Conclusions

In the present work, various foams based on flax gum-filled epoxy resin were produced and two foam-based and short flax fiber-reinforced composites were developed. The microstructural analysis highlighted the influence of the chemical modifications on the internal structuring of the pore networks and material porosity. The mechanical analysis showed how the oxidation of the gum resulted in higher stiffness and strength values. This is attributed to better hardening due to the oxidation of the flax gum. The incorporation of epoxy resin and short flax fibers induced a significant decrease in mechanical performance even when the oxidized gum was considered. In addition, the incorporation of flax fibers at 48% did not change the stiffness but, very interestingly, significantly increased the cohesion and bio-based content of the composite. As expected, the thermal properties were correlated with the material's density and porosity, and the results are consistent with the current literature. These results are promising for using flax gum as a filler in composites, and the modulation of the gum and fiber contents should be investigated to optimize the overall performance of the materials.

Supplementary Materials: The following supporting information can be downloaded at: https://www.mdpi.com/article/10.3390/jcs8070244/s1, Figure S1: FTIR spectra of (A) native and oxidized Flax gum; (B) Flax fibres (F1 and F1ox); Figure S2: FTIR spectra of (A) Oxidized Flax gum filled epoxy filled foams (FGox-80 and FGox-20); (B) composites FG-Comp and FGox-Comp; Figure S3: SEM images of the cross-section morphology of composites.

Author Contributions: C.M.: Methodology, Validation, Investigation; M.Z.: Methodology, Investigation, Formal analysis, Writing—Original Draft; M.D.: Investigation, Writing—Original Draft; Y.A.: Investigation; N.N.: Supervision, Writing—Original Draft; A.B.: Writing—Original Draft; D.B.: Supervision, Writing—Original Draft; F.D.: Conceptualization, Supervision, Project administration, Funding acquisition, Writing—Original Draft. All authors have read and agreed to the published version of the manuscript.

Funding: This research was funded by Region Hauts-de-France and Van Robaeys Frères.

Data Availability Statement: The data are available on demand.

Acknowledgments: The authors graciously acknowledge Steven Ruellan, Bastien Watbled, and Camille Galand.

Conflicts of Interest: The authors declare no conflicts of interest. The funders had no role in the design of the study; in the collection, analyses, or interpretation of the data; in the writing of the manuscript; or in the decision to publish the results.

References

1. Ngo, T.D. Natural Fibers for Sustainable Bio-Composites. *Nat. Artif. Fiber-Reinf. Compos. Renew. Sources* **2018**, *3*, 107–126.
2. Rouilly, A.; Vaca-Garcia, C. *Bio-Based Materials. Introduction to Chemicals from Biomass*, 2nd ed.; Clark, J., Deswarte, F., Eds.; John Wiley & Sons, Ltd.: Hoboken, NJ, USA, 2015.
3. Shah, D.U. Developing plant fiber composites for structural applications by optimizing composite parameters: A critical review. *J. Mater. Sci.* **2013**, *48*, 6083–6107. [CrossRef]
4. Chen, J.; Nichols, B.; Norris, A.; Frazier, C.E.; Edgar, K.J. All-polysaccharide, self-healing injectable hydrogels based on chitosan and oxidized hydroxypropyl polysaccharides. *Biomacromolecules* **2020**, *21*, 4261–4272. [CrossRef] [PubMed]
5. Azeredo, H.M.C.; Waldron, K.W. Crosslinking in polysaccharide and protein films and coatings for food contact—A review. *Trends Food. Sci. Technol.* **2016**, *52*, 109–122. [CrossRef]

6. Varma, A.J.; Jamdade, Y.K. On the Dual Role of Starch, Cellulose and their Dialdehydes as Fillers and Accelerators in the Tertiary Amine Catalysed Curing of Epoxy Resin. *Carbohydr. Polym.* **1985**, *5*, 309–316. [CrossRef]
7. Hassan, N.A.A.; Ahmad, S.; Chen, R.S.; Natarajan, V.D. Synergistically enhanced mechanical, combustion and acoustic properties of biopolymer composite foams reinforcement by kenaf fiber. *Comp. Part A* **2022**, *155*, 106826. [CrossRef]
8. Yang, K.; Zhang, Z.; Liu, Y.; Li, S.; Chen, D.; Li, Z. Biomass-based porous composites with heat transfer characteristics: Preparation, performance and evaluation—A review. *J. Por. Mater.* **2002**, *29*, 1667–1687. [CrossRef]
9. Wei, X.; Ding, S.; Liu, S.; Yang, K.; Cai, J.; Li, F.; Wang, C.; Lin, S.; Tian, F. Polysaccharides-modified chitosan as improved and rapid hemostasis foam sponges. *Carbohydr. Polym.* **2021**, *264*, 118028. [CrossRef] [PubMed]
10. Mello, L.R.P.F.; Mali, S. Use of malt bagasse to produce biodegradable baked foams made from cassava starch. *Ind. Crops Prod.* **2014**, *55*, 187–193. [CrossRef]
11. González-García, S.; Hospido, A.; Feijoo, G.; Moreira, M.T. Life cycle assessment of raw materials for non-wood pulp mills: Hemp and flax. *Res. Conserv. Recycl.* **2010**, *4*, 923–930. [CrossRef]
12. Soykeabkaew, N.; Supaphol, P.; Rujiravanit, R. Preparation and characterization of jute- and flax-reinforced starch-based composite foams. *Carbohydr. Polym.* **2004**, *58*, 53–63. [CrossRef]
13. Ramesh, M. Flax (*Linum usitatissimum* L.) fibre reinforced polymer composite materials: A review on preparation, properties and prospects. *Prog. Mat. Sci.* **2019**, *102*, 109–166. [CrossRef]
14. Musa, C.; Kervoëlen, A.; Danjou, P.-E.; Bourmaud, A.; Delattre, F. Bio-based unidirectional composite made of flax fibre and isosorbide-based epoxy resin. *Mater. Lett.* **2020**, *258*, 126818. [CrossRef]
15. Alix, S.; Marais, S.; Morvan, C.; Lebrun, L. Biocomposite materials from flax plants: Preparation and properties. *Comp. Part A* **2008**, *39*, 1793–1801. [CrossRef]
16. Paynel, F.; Pavlov, A.; Colasse, L.; Rihouey, C.; Follain, N.; Duriatti, D.; Bizet, L.; Allan, I.; Lebrun, L.; Marais, S.; et al. Preparation and characterization of flax biocomposites made of seed mucilage reinforced by fibers. *Comp. Part A* **2015**, *69*, 299–305. [CrossRef]
17. Cui, W.; Mazza, G.; Biliaderi, C.G. Chemical structure, molecular size distribution and rheological properties of flaxseed gum. *J. Agric. Food Chem.* **1994**, *442*, 1891–1895. [CrossRef]
18. Olsson, E.; Menzel, C.; Johansson, C.; Andersson, R.; Koch, K.; Järnström, L. The effect of pH on hydrolysis, cross-linking and barrier properties of starch barriers containing citric acid. *Carbohydr. Polym.* **2013**, *98*, 1505–1513. [CrossRef] [PubMed]
19. Kato, Y.; Matsuo, R.; Isogai, A. Oxidation process of water-soluble starch in TEMPO-mediated system. *Carbohydr. Polym.* **2003**, *51*, 69–75. [CrossRef]
20. Sbiai, A.; Maazouz, A.; Fleury, E.; Sautereau, H.; Kaddami, H. TEMPO-Mediated Oxidation of Lignocellulosic Fibers from Date Palm Leaves. *Carbohydr. Polym.* **2012**, *86*, 149–186. [CrossRef]
21. Blumenkrantz, N.; Absoe-Hansen, G. New methods for quantitative determination of uronic acids. *Anal. Biochem.* **1973**, *54*, 484–489. [CrossRef]
22. Da Silva Perez, D.; Montanari, S.; Vignon, M.R. TEMPO-mediated oxidation of cellulose III. *Biomacromolecules* **2003**, *4*, 1417–1425. [CrossRef] [PubMed]
23. Feldkamp, L.A.; Davis, L.C.; Kress, J.W. Practical cone-beam algorithm. *J. Opt. Soc. Am.* **1984**, *1*, 612–619. [CrossRef]
24. Schneider, C.A.; Rasband, W.S.; Eliceiri, K.W. NIH Image to ImageJ: 25 years of image analysis. *Nat. Methods* **2012**, *9*, 671–675. [CrossRef] [PubMed]
25. Arzt, M.; Deschamps, J.; Schmied, C.; Pietzsch, T.; Schmidt, D.; Tomancak, P.; Haase, R.; Jug, F. LABKIT: Labeling and Segmentation Toolkit for Big Image Data. *Front. Comput. Sci.* **2022**, *4*, 777728. [CrossRef]
26. Zaidi, M.; Baillis, D.; Naouar, N.; Depriester, M.; Delattre, F. Thermal Conductivity and Microstructure of Novel Flaxseed-Gum-Filled Epoxy Resin Biocomposite: Analytical Models and X-ray Computed Tomography. *Materials* **2023**, *16*, 6318. [CrossRef]
27. *ASTM Standard D1621*; Standard Test Method for Compressive Properties of Rigid Cellular Plastics. ASTM International: West Conshohocken, PA, USA, 2004.
28. *ASTM Standard D7984-21*; Standard Test Method for Measurement of Thermal Effusivity of Fabrics Using a Modified Transient Plane Source (MTPS) Instrument. ASTM International: West Conshohocken, PA, USA, 2021.
29. Wojtasik, W.; Kulma, A.; Kostyn, K.; Szopa, J. The changes in pectin metabolism in flax infected with Fusarium. *Plant Phys. Biochem.* **2011**, *49*, 862–872. [CrossRef]
30. Dubois, F.; Musa, C.; Duponchel, B.; Tifahy, L.; Sécordel, X.; Mallard, I.; Delattre, F. Nuclear magnetic resonance and calorimetric investigations of extraction mode on flaxseed gum composition. *Polymers* **2020**, *12*, 2654. [CrossRef]
31. Petera, B.; Delattre, C.; Pierre, G.; Wadouachi, A.; Elboutachfaiti, R.; Engel, E.; Poughon, L.; Michaud, P.; Fenoradosoa, T.A. Characterization of arabinogalactan-rich mucilage from *Cereus triangularis* cladodes. *Carbohydr. Polym.* **2015**, *127*, 372–380. [CrossRef] [PubMed]
32. Liu, X.; Renard, C.M.G.C.; Bureau, S.; Le Bourvellec, C. Revisiting the contribution of ATR-FTIR spectroscopy to characterize plant cell wall polysaccharides. *Carbohydr. Polym.* **2021**, *262*, 117935. [CrossRef]
33. Borkotoky, S.S.; Ghosh, T.; Bhagabati, P.; Katiyar, V. Poly (lactic acid)/modified gum arabic (MG) based microcellular composite foam: Effect of MG on foam properties, thermal and crystallization behavior. *Int. J. Biol. Macromol.* **2019**, *125*, 159–170. [CrossRef]
34. Paladini, G.; Venuti, V.; Crupi, V.; Majolino, D.; Fiorati, A.; Punta, C. FTIR-ATR analysis of the H-bond network of water in branched polyethyleneimine/TEMPO-oxidized cellulose nano-fiber xerogels. *Cellulose* **2020**, *27*, 8605–8618. [CrossRef]

35. Nie, J.; Mou, W.; Ding, J.; Chen, Y. Bio-based epoxidized natural rubber/chitin nanocrystals composites Self-healing and enhanced mechanical properties. *Comp. Part B* **2019**, *172*, 152–160. [CrossRef]
36. Ferreira, E.S.; Rezende, C.A.; Cranston, E.D. Fundamentals of cellulose lightweight materials: Bio-based assemblies with tailored properties. *Green Chem.* **2021**, *23*, 3542–3568. [CrossRef]
37. Liu, P.; Li, X.; Min, P.; Chang, X.; Shu, C.; Ding, Y.; Yu, Z.Z. 3D lamellar-structured graphene aerogels for thermal interface composites with high through-plane thermal conductivity and fracture toughness. *Nano-Micro Lett.* **2021**, *13*, 22. [CrossRef] [PubMed]
38. Zhang, G.; Chen, H.; Yang, S.; Guo, Y.; Li, N.; Zhou, H.; Cao, Y. Frozen slurry-based laminated object manufacturing to fabricate porous ceramic with oriented lamellar structure. *J. Eur. Ceram. Soc.* **2018**, *38*, 4014–4019. [CrossRef]
39. Prado, N.S.; Silva, I.S.V.D.; Silva, T.A.L.; Oliveira, W.J.D.; Motta, L.A.D.C.; Pasquini, D.; Otaguro, H. Nanocomposite films based on flaxseed gum and cellulose nanocrystals. *Mater. Res.* **2018**, *21*, e20180134. [CrossRef]
40. Valette, V.; Kébir, N.; Tiavarison, F.B.; Burel, F.; Lecamp, L. Preparation of flexible biobased non-isocyanate polyurethane (NIPU) foams using the transurethanization approach. *React. Funct. Polym.* **2022**, *181*, 105416. [CrossRef]
41. Peyrton, J.; Avérous, L. Structure-properties relationships of cellular materials from biobased polyurethane foams. *Mater. Sci. Eng. Rep.* **2021**, *145*, 100608.
42. Ambli, K.G.; Dodamani, B.M.; Jagadeesh, A.; Vanarotti, M.B. Heterogeneous composites for low and medium temperature thermal insulation: A review. *Energy Build.* **2019**, *199*, 455–460. [CrossRef]
43. Kymäläinen, H.R.; Sjöberg, A.M. Flax and hemp fibres as raw materials for thermal insulations. *Build. Environ.* **2008**, *43*, 1261–1269. [CrossRef]